Friday 27th May 2022

Ae105c: Space Engineering

Proposal for Space Solar Power System for Maui, HI

Olivia Ernst, Maximilian Adang, George Popov, Divesh Soni

Graduate Aerospace Laboratories of the California Institute of Technology
Instructor: Professor Pellegrino
TA: Alexander Wen

Version Control

Revision	Description	Date
1	Draft Proposal	May 12, 2022
2	Final Proposal	May 27, 2022

Acronyms

ADCS	Attitude Determination and Control System
CDH	Command and Data-Handling
COMM	Communications Subsystem
COTS	Component-Off-The-Shelf
EGSE	Electrical Ground Support Equipment
EPS	Electrical Power Supply
EM	Electromagnetism
FMG	Fault Management Subsystem
IMU	Inertial Measurement Unit
JPL	Jet Propulsion Laboratory
LEO	Low Earth Orbit
MCU	Microcontroller Unit
MLI	Multi-Layer Insulation
MSS	Mobile Satellite Surface
NASA	National Aeronautics and Space Administration
PLD	Payload Subsystem
PROP	Propulsion System
PWR	Power Subsystem
SoOp	Signals-of-Opportunity
SWE	Snow Water Equivalent
SWI	Soil Water Index
STR	Structures & Mechanisms Subsystem
SYS	System
S/C	Spacecraft
THM	Thermal Subsystem
TRL	Technology Readiness Level
TVAC	Thermal Vacuum
UNP	University Nanosatellite Program
V&V	Verification and Validation

Contents

List of Figures

List of Tables

1 Purpose and Background

The Sun is the greatest source of untapped energy on Earth. While solar power on the surface of the Earth is limited by daylight hours, power station storage capacities, and favorable weather conditions at the solar power plant, space solar power (SSP) is a technology that sidesteps many of the challenges of implementing continuous solar power generation on the ground by elevating the power collector to space, ideally mitigating the challenges of day/night cycle, favorable weather conditions, and land necessary for solar farms. Deploying the first cost-competitive and reliable SSP infrastructure by 2032 is a challenge driven by the technological maturity of the baseline components and the fundamental limits of orbital spacecraft. Maui, HI requires a baseload power requirement of 100MW supplied continuously to the island by the planetside power plant. A reliable and cost competitive architecture will need to function for 20 years at a cost of $0.35 - $0.25 / kWh. The top level objectives of the SSP architecture are thus defined as follows:

1. Generate 100MW continuously at the ground station
2. Deploy the architecture by 2032
3. Operate reliably and competitively for 20yr
4. Cost $0.25 - $0.35 / kWh

These top level objectives drive the functional requirements of the space segment of the SSP architecture. The fundamental limits on power transmission efficiency between the spacecraft and the ground station require order-of-magnitude greater power collection by the spacecraft for the ground station to receive enough power to distribute 100MW continuously. Solar panel photovoltaic (PV) efficiencies drive the size of the solar collection surface in space, while the physical limitations on launchable solar panel size determine the number of launches necessary to construct the SSP in orbit. The architecture proposed hereafter is an end to end solution to the top level objectives derived from the technological constraints on a space solar power system.

2 Considered Architectures

2.1 SPS Alpha

This concept[16] is proposed under NASA Grant NNX11AR34G. The goal is to investigate space solar power and deliver energy to Earth. Analogous to a colony of ants, a very large number of modules will get assembled on orbit to form a large satellite(Figure-1). Power collection will be done with a large number of sunlight intercepting reflectors mounted on a non moving structure. These will be connected to a very large primary array of transmitters with the help of a truss structure. The transmitters will point towards the nadir to send the power to the Earth station.

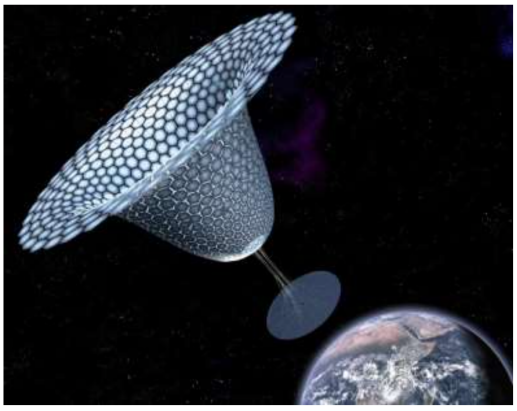

Figure 1: One of the proposed versions for SPS-ALPHA concept.

The key aspects of this design are summarized as follows:

- RF retrodirective phased arrays
- High efficiency solid state amps
- Autonomous robotics on orbit
- Special shape for gravity gradient stabilization
- No slew required in design
- Claim: 20¢ per kWh for 100 MW

There are a few challenges and shortcomings which come along this proposal. Considering the shape of the space segment, it is inefficient with daily and seasonal solar variation. For example, the other side of the reflectors will be a passive area in space. This can be prevented with designing a shape with dual sided functionality. Another challenging aspect of this design is the large assembly of modules on orbit. The proposal estimates requiring hundreds of astronauts and thousands of robots for the construction of the space modules.

2.2 Power Star

This concept[17] has a spherical power collection module of a diameter ≈ 1km on orbit which is made with printed solar cells and microwave transmitters. Ground stations receive power with arrays of rectifying antennas.

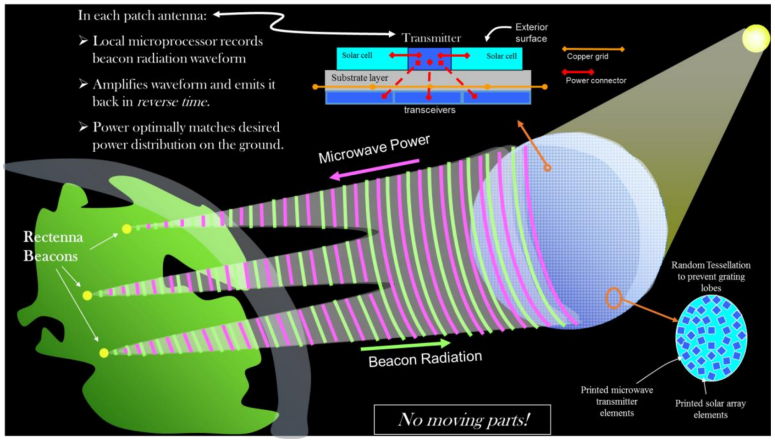

Figure 2: Power star operation overview.

The primary features of the concept are as follows:

- A sphere with random tessellations
- No moving parts
- Printed SA and transmitter patches
- Power beam control with multiple spots
- Proposed GEO orbit
- Ideal λ =10cm with a rectenna size on ground of 3.5km
- Using an ECHO satellite technique to launch and inflate on orbit

2.3 Caltech Baseline

This concept is based on a flat plate based power collection architecture. Multiple spacecrafts will beam the power collected on orbit towards a series of ground stations spread over Earth. They will undergo slew maneuvers depending on which orbit the mission will be finalized into. Investigation on MEO orbits for such architecture has been extensively done.[18]

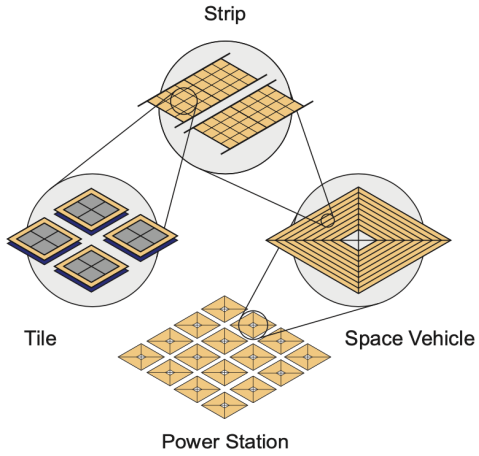

Figure 3: A flat panel power collection scheme.

Following are the major features of this concept:

- Individual phased arrays on 60m x 60m spacecraft
- GEO or MEO options explored
- Single or double sided PV and transmitter design
- RF proposed as wavelength
- Folding pattern to fit into a manifold and then deploy at orbit
- Lightweight booms and longerons to support deployed PV area

3 Trade studies

3.1 Orbit selection

This section describes the orbit selected for the implementation of the SSP architecture. The first significant requirement of the project is to provide 100MW continuously to the island of Maui. The orbit selection is crucial to the manner in which this requirement is satisfied, involving the relationship between the space segment (power collection on-orbit) and ground segment (power reception from space segment and distribution to Maui). The primary driving requirement of the orbit choice assuming the use of photovoltaics (PV) is the necessary area in orbit to collect enough power to have 100MW at the ground station. Due to compounding system efficiencies, an order of magnitude greater power (3.39 GW) must be collected on orbit for the ground station to be able to distribute 100MW. This necessitates an area of PV (2.49 km^2) that must be constantly transmitted to the ground station for the power distribution to be continuous.

3.2 GEO Orbit

Geostationary orbit presents an obvious choice by tying the location of the space segment to the location of the ground segment, reducing the complexity of orbital maneuvers, mitigating power interruptions in the form of eclipses, and ensuring nearly continuous power transfer from the space

segment to the ground segment. This option minimizes the total time (82 hr / yr) that the space segment is fully eclipsed from the ground segment, and reduces the power loss that the ground segment must be robust to in order to maintain continuous 100MW of power distribution to Maui. Using conventional solar panels and a spacecraft orientation-fixed transmitter, a spacecraft must maintain its orientation such that its transmitter points towards the ground station at all times. Given that a phased-array transmitter may overcome this pointing requirement to a certain degree Figure-9, the spacecraft experiences a cyclic efficiency maximum and minimum as the spacecraft's pointing drifts from the ground station and the phased array compensates. This phenomenon results in a conventional "single PV layer sandwich structure" photovoltaic and transmitter combination maneuvering twice per day, one large continuous slew between squint angles of 76° and -76° and one short slew while the space segment is at local midnight 3.3.

Medium Earth orbit (MEO) presents a less obvious option where the primary benefit is a reduction in the necessary transmitter power, size, and potentially even cost. MEO has a shorter orbital period than one day, which means that maintaining continuous power transmission in MEO requires continuous flybys of satellites, dramatically increasing the overall number of satellites. This increase is nearly 2x at the optimal orbital altitude where GPS signals are available for satellite constellation coordination, enabling formation flying or docking. The Van Allen radiation belts also complicate this choice, resulting in only a few viable sections for constellation placement. Satellite longevity is also reduced in these areas, as most rad-hardened electronics are capable of withstanding 15 years of continuous radiation bombardment, but the project must last 20 years. While options near GEO exist, this orbit does not benefit significantly more from extremely high positional resolution from GPS satellites, and suffers from an increase in satellites over the GEO option, which would require the same launch costs anyway.

The low Earth orbit (LEO) configuration exhibits more dramatic versions of the same beneficial and detrimental characteristics of MEO. The number of satellites that must be launched becomes extreme, requiring more launches than feasible. There are also significant atmospheric disturbance forces that would be very difficult to deal with. Thus, GEO and MEO were the two prevailing options worthy of pursuing a detailed trade study on.

We note here that a constellation of satellites is highly beneficial for SSP implementations designed to power *multiple* ground stations. Deploying many more satellites than can be overhead transmitting power is a highly inefficient configuration for the purposes of powering a single ground station.

Criteria	**GEO**	**MEO**
Number of spacecraft	692	2,034
Radiation accumulation over 20 years (Mrads)	0.63%	6.3%
Ground station rectenna size (km^2)	8.6	2.37
Number of launches	139	407

Table 1: Orbit Trade study

The primary driving factor in the consideration of these three orbits is the required area of PV and transmitters (2.49 km^2), which in turn drives the quantity of component spacecraft and thus the cost and timeline of the project. We note that the use of solar concentrators reduces this overall area of photovoltaic depending on their structural configuration, but maintaining a given orbit and trading traditional PV for concentrators demands the same transmitter and structural area, and thus the same overall number of spacecraft. There are also similar thermal limits to using solar concentrators. Choosing a lower orbit that *also* reduces the necessary transmitter area does not overcome this challenge, as the spacecraft increase is 2.57x, while the reduction in ground station rectenna area due to a combination of these changes 71.32 % for a satellites placed at about 20000 km. This reduction in area does not appreciably reduce the projected cost of the architecture and more importantly, does not affect the cost or feasibility of the system. Furthermore, choosing to collect far *greater* than the requisite 3.39 GW on-orbit for discontinuous power transmission to charge batteries at the ground station does not alter the choice of orbit. This option logically requires an *increase* in

the number of satellites that must fly overhead. While pursuing this option may have merit, choosing any of these three alternate configurations relies on technology with lower TRL and feasibility than the single PV layer sandwich structure.

Orbital Period (h)	11.17
Sunlight Time	10.27
Eclipse Time	0.9
Transmission Time	4.34
Orbital Velocity (km/s)	3.96
Eclipse Time per half-year	707.78
Transmission time per half-year	3406.67

Table 2: MEO Orbit Characteristics

Therefore, a GEO orbit was selected for the SSP. This configuration sees its component satellites overhead at all times, maintaining pointing to the ground station.

3.3 Power collection

3.3.1 Solar cells

This section describes the solar cell options considered to collect power on orbit. Only market available options are considered. A trade study between high efficiency Si cells, Self curing Si cells, Triple Junction cells(3J) and Quadruple Junction cells(4J) is shown in Table-4. Metrics like BOL and EOL efficiencies, power per meter square of the cell, power per kg of the cell, and thickness of the bare cell are considered for the comparison. Data from the available research[19][20][5] and specification sheets from the manufacturer are used. A worst case sun incidence angle of 10^o and a distribution efficiency(η_d) of 90% is assumed to calculate the power figures. The costs are inflation adjusted from a 2000 study.[21].

Criteria	**Conventional Si[1]**	**Self curing Si-20µm**[4]	**Triple Junction[2]**	**Quadruple Junction[3][22]**
Weight(kg/m^2)	0.32	0.05	0.86	0.5
BOL efficiency	16.9%	20%	30%	32%
EOL efficiency[19](GEO @60^{o}C, 1MeV, 5E14 e/cm^2	12.5%	19%	28.1%	29.7%
Thickness(µm)	160	20	170	120
Power_BOL(W/m^2)	205	273.2	358	386
Power_BOL(W/kg)	641	-	416	772
Cost(k$/m^2)[21]	22.5	-	149.6	179.52

Table 3: Solar cell Trade study

Beginning of Life (BOL) efficiencies are obtained from the specification sheet. End of life or EOL efficiencies are calculated based on projected degradation from the available literature[23]. One of the EOL metrics used within industry to establish degradation time is a fluence of 1 MeV of electrons when in GEO orbit. This is equivalent to different mission times on orbit[24] with 10 years for Si cells and 33 years for 3J GaAs cells.

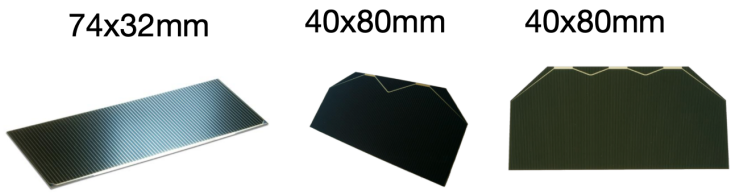

Figure 4: From left to right, 3mm-Si cell[1], 3J GaAs cell[2] and 4J GaAs[3] cells from Azurespace.

It is fairly clear that 4J cells are superior with regards to efficiencies, thickness and power. These require a metamorphic cell design and show extraordinary radiation hardness for voltage and current similar to 3J GaAs cells[20]. 3J cells are not selected because of high weight per square meter compared to Si cells. Moreover, 4J cells are discarded because of the amount of cost increase is enormous compared to gain in efficiencies or reduction in mass.

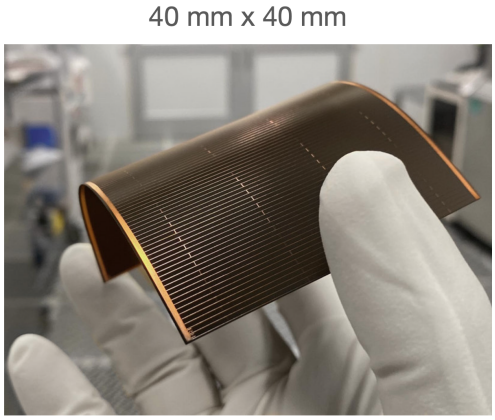

Figure 5: 20µm-Si cell[4] from Solestial.

It can be estimated that for a mission life of 20 years, the efficiency of a 3J GaAs cell drops from 0.31 to 0.11 effectively because of the yearly degradation of 2.5% and inherent degradation of 0.8[24]. Hence, the EOL efficiency is the prime factor in this trade which is directly related to radiation tolerance. Various advances have been made in increasing radiation tolerance of the conventional Silicon based cells[25]. It is reported that the p-type base Silicon solar cells exhibit higher radiation tolerance when compared to the n-type. Moreover, a lower carrier concentration (higher base resistivity) is crucial for better performance at the end of life. As a result, 20µm Silicon based solar cells are selected which have a capability to self cure the radiation damage. They are manufactured with new techniques in the area of wafer defect engineering. Literature studies have also confirmed the efficiency numbers claimed for 40µm thick Si solar cells[26].

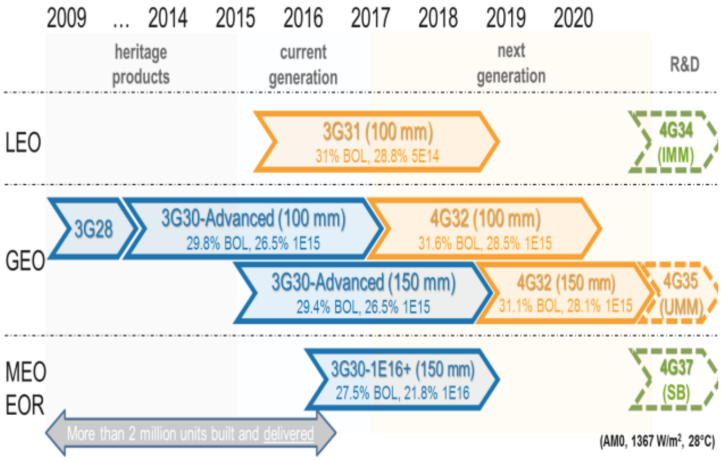

Figure 6: Product roadmap of AZURSPACE for three market segments. Colours indicate cell technology: lattice- matched (blue), UMM (orange), inverted metamorphic (IMM, green) or semiconductor bonded (SB, green)[5]

A projected value of the solar cell BOL efficiencies can be obtained for 2030 considering a similar trend as shown in Figure-6. BOL numbers saw an increment from 29.8% to 31.6% from 2009 to 2020 for GEO platform. Assuming an assembly time of 2 years for solar arrays, a projection of 21.8% BOL efficiencies for Silicon cells in 2030 is quite reliable. This data will be used in Table-11 in Section-6.1.

3.3.2 Solar cell advanced technology considerations

This section describes additional considerations for solar cells with more advanced technologies. Primary criteria for a comparative analysis include required area of objects in orbit, thermal management, and non-recurring engineering costs. Considered options include single-sided, double-sided, and solar concentrators.

Criteria Solar Technology	**Single-sided PV (selected)**	**Solar Concentrator [27]**	**Double-sided PV**
Efficiency	0.20	0.98	0.20
PV subsystem specific power (kW/kg)	1.05	4.30	0.53
Required PV area (km^2)	2.49	0.166	3.55
Number of slews per orbit	2	2	2 (instantaneous)
Thermal management	Little/None	Critical	Little/None
NRE Costs	None	Prohibitive	Costly

Table 4: Solar cell Advanced Tech Trade study

Solar concentrators appear to be a very promising addition to the system design. Although concentrators can reduce the amount of PV area, the required radiator area to provide necessary thermal management will return overall area to the original requirement for single-sided PV. In addition, any failure in the thermal management system for a solar concentrator design will significantly reduce the efficiency of the power transmission system. A 15 C increase from the specified operating temperature can reduce efficiency by as much as 6% [28]. The final reason concentrators were not selected is due to prohibitive non-recurring engineering costs associated with developing this technology. Double-sided PV does not appear to be a reasonable choice for the design. Double-sided PV would require about 1.5 times the amount of PV, which means 1.5 times the cost. This increased mass would in turn increase propulsion requirements for slew maneuvers and disturbance control. In addition, this would require

the development of RF transparent PV. For these reasons, the existing single-sided PV technology was selected for the architecture.

3.4 Launch Vehicle selection

This section describes the considerations made when determining the optimal launch vehicle to transfer the space segment to the chosen orbit. The inverse scaling of space segment satellite number to orbital altitude is not outweighed by potential savings costs for launching satellites to lower orbits due to the sizeable increase in required number of launches. The choice to use the thin Si photovoltaics with some flight heritage instead of developing solar concentrator technology increased the projected mass of the space segment. This placed strict requirements on the capabilites of the launcher chosen, as it must be able to launch 692 satellites in less than 200 launches total, which is the estimated total number of launches over 5 years assuming SpaceX continues a trend of increasing number of rockets launched per year over 5 years by $30\tilde{\%}$, leading to a launch capability of $4\tilde{0}$ rockets per year [29]. The number of launches was determined using a combination of the available volume and the mass capabilities of the launcher. Starship has a projected payload of 100 metric tons GTO, and a payload fairing diameter of 9m and height of 18m. This results in a conservative estimate of < 25 satellites per launch, mass limited significantly by the 3 ton weight of each spacecraft.

Criteria	**Falcon 9**	**Ariane 5**	**Starship**
Number of Launches	139	173	8
Risk	Available	Available	Unknown
Cost-to-Launch	$60 million	$177 million	$2 million

Table 5: Launcher Trade study

The trade weighs heavily in favor of using the Starship vehicle, which is designed to launch numerous and massive satellites into orbit and beyond. This choice at the cited price point of $2 million per launch might even reduce the projected cost to launch to a lower orbit. However, Starship has not yet demonstrated orbital capabilities, and it is a risky proposition to design based on an as-of-yet unproven launch vehicle. This choice would decrease the overall feasibility of the proposed SSP architecture. Therefore, the decision was made to design the architecture around a proven launch vehicle, the Falcon 9 launcher. This launch vehicle is capable of lifting 5 satellites per launch, resulting in a final total of 139 launches and an overall cost of 8.3 billion. Starship would be significantly more efficient both in terms of time and cost, with an overall cost of 16 million and only 8 launches. These costs do not factor in mission specific costs such as satellite deployment structures or launch vehicle maintenance/production costs resulting from such large numbers of launches. Starship remains an excellent choice provided its reliability and availability by 2030. The option to use Starship should remain open in the future, as its *projected* capabilities significantly increase the feasibility of this project.[30][31]

3.5 Power Transfer

This section describes the considerations surrounding which wavelength to transmit at the power collected by the photovoltaics. Higher wavelengths have lower energy densities, and thus lower the efficiency of transmission in our system. Our options are overall limited by the transmission windows that Earth's atmosphere allows. The 3 main windows are located at the visible light spectrum, the infrared spectrum, and at radio frequencies. Given that there are very serious concerns surrounding a 100+ MW IR or visible light laser beaming the Earth, and that both of them tend to be quite weather dependent for their atmospheric transmission efficiencies, we are forced to choose to use radio frequencies, and we use the lowest wavelength available in the transmission window, which is about 5 GHz.

Wavelength	**0.5 um Visible light/Laser**	**10 um IR**	**6 cm RF (selected)**
Atmospheric Loss at Mauna Kea	2-10%	5-10 %	<1%
Safety concerns	Severe	Severe	Minor
Energy Density	Optimal	Near optimal	Least energy density
Other considerations	Highly weather dependent, cloud scattering	Weather dependent	

Table 6: Power Transfer Trade study

3.6 Docking vs Formation Flying

This section describes the considerations made between choosing to formation fly or dock the hundreds of component spacecraft that make up the space segment of the SSP architecture. As previously described, the scale of the space segment of the SSP demands more mass and volume than can be lifted to orbit in a single launch. This requirement thus necessitates the question of how to configure these numerous components. Both docking and formation flying the component spacecraft provide configurations with projected comparable results. With the goal of designing the system most feasible to deploy by 2032, options such as on-orbit manufacturing and robotic self assembly that were more complex than docking were discounted due to their low TRL. Demonstrating TRL 6 for these options by 2030 would add on non-recurring engineering cost and reduce the plausibility of this architecture. Therefore, docking and formation flying were the two most feasible options considered for a full trade study.

Spacecraft docking and formation flying both require robust ADCS components and state-of-the-art controls algorithms to ensure the success and safety of the architecture. Docking the spacecraft provides a greater level of certainty in the idealized transmission efficiency due to definite spacing between the phased transmitter arrays. Additionally, docking the spacecraft reduces the mass of the spacecraft bus, as propellant for 20 years of station keeping and precise attitude control is no longer necessary in this configuration. However, this configuration requires added mass in the form of docking components, potentially offsetting the reduction mass from lacking station keeping propellant. Furthermore, this configuration is not robust to many component failures. Should individually docked spacecraft fail, there is little recourse for excising the failed spacecraft safely, and updating the structure with additional component spacecraft would likely need to be done from the outside of the structure. While spacecraft failing prior to docking is ostensibly as unsafe as a formation flying configuration, the latter configuration leverages the avionics, power, and ADCS components necessary for both options in a more efficient, feasible, and robust manner. Ultimately, this trade was conducted at the level of feasibility because the similarities between the individual spacecraft at a component level are so similar.

Criteria	**Docking**	**Formation Flying (selected)**
Controllability	- Converge orbital states with MPC - Full structural rigidity and control	- Must maintain power optimal spacing with accuracy of $\lambda/2$ GPS (3m spacing only)
Demonstrated Feasibility	- Docking between small numbers of structures	- LEO formation flying with spacing on the order of meters
Risk	- Effective Single Point of Failure once docked	- High risk during slewing
Complexity	- Docking interface rigidity and added mass	- Spacecraft to spacecraft communication (3 axis optical ranging)

Table 7: Docking vs Formation Flying Trade study

The configuration of the architecture is by far the most technologically challenging aspect of the SSP. Docking and formation flying are the two most feasible choices for achieving coherent power transfer from space to the ground segment, and yet both options rely on technology that has not been demonstrated at the scale of this project. Formation flying was selected due to the greater feasibility of its most challenging features (high resolution positioning and rangefinding), and less risky implementation. The formation flying configuration is robust to multiple spacecraft failures, and doesn't introduce uncertainties in the structural integrity as a result of docking hundreds of component spacecraft into a megastructure on the order of kilometers long and wide. Finally, formation flying also helps deal more efficiently with any individual spacecraft failure.

4 Space power station architecture

The SSPP architecture presented here satisfies the requirements of the request for proposal while mitigating inherent risks of a space solar power station. The architecture is designed around EOL PV efficiencies to ensure operation for 20 years, supplying 101.2MW of power continuously at EOL, and 112.13 MW continuously at BOL. After ground station conversion inefficiencies, this translates to 100MW supplied to the Maui power grid, and 1.2MW supplied to battery storage banks at the ground station to ensure continuous power supply during eclipse seasons and local midnight. This system is designed with technology readily available by 2030, relying on commercially available thin Silicon PV cells with space qualification, existing space-based phased array and ground based dipole rectennas, and the Falcon 9 launch vehicle. The main component of the architecture requiring further technological development is the formation flying of the component spacecraft. This has not been demonstrated on the scale of hundreds of spacecraft, but relies on sensor configurations and algorithms with flight heritage for 2 spacecraft flying formation. Spacecraft propulsion will be performed with pulsed plasma thrusters with high reliability, low propellant mass, and sufficient propellant and power for 20 years of operation. All electronics are designed with standard space-based radiation hardened components, capable of withstanding an accumulated 0.63 Mrad over the 20 years of life.

4.1 Flight system concept and analysis of selected orbit(s)

The space solar power project presented here will provide 100 MW of power to the island of Maui, HI continuously for 20 years. The overall cost shall be price competitive to space solar supply, and not exceed $0.25/kWh. The system deployment will begin in 2030 and will be completed in 2032.

Following are the major features of this concept:

Space solar power has several advantages over ground based systems. Space power is immune to inclement weather and the day/night cycle. Satellite based solar power stations collect and transmit more energy, as there is 1.36x solar intensity outside of the Earth's atmosphere.

A GEO orbit was selected for the proposed architecture due to the requirement to only supply power to a single ground station at Maui and the goal of minimizing the overall number of spacecraft. While a MEO orbit makes sense for SSP architectures supplying power across the world, supplying power to a single location reduces the efficiency of such an approach drastically through massive increase in satellite numbers required to provide sufficient power continuously to Maui. Power collection transmission occurs uninterrupted except during an eclipse. Considering all efficiency losses presented in Table 11 with RF-to-DC conversion, the total power collected after considering space transmission inefficiencies is 139.4 MW. Eclipses occur twice a year in GEO throughout a 41 hour time block. In order to send power continuously, the satellite system will need to transmit 101.2 MW of power. 100 MW will continuously be sent directly to Maui, and 0.98 MW (post inefficiencies) will go into energy storage. The power sent to storage already incorporates a 90% efficiency of depositing and withdrawing energy from the batteries.

Power transfer will occur in the RF range, with a selected wavelength of 6 cm or transmission frequency of 5 GHz. The spacecraft will deploy to dimensions of 60 x 60 m, and requires 692 spacecraft to reach the PV area required to transmit sufficient power. The spacecraft will be launched on the Falcon 9, and it will take 3 years to achieve a total of 139 launches.

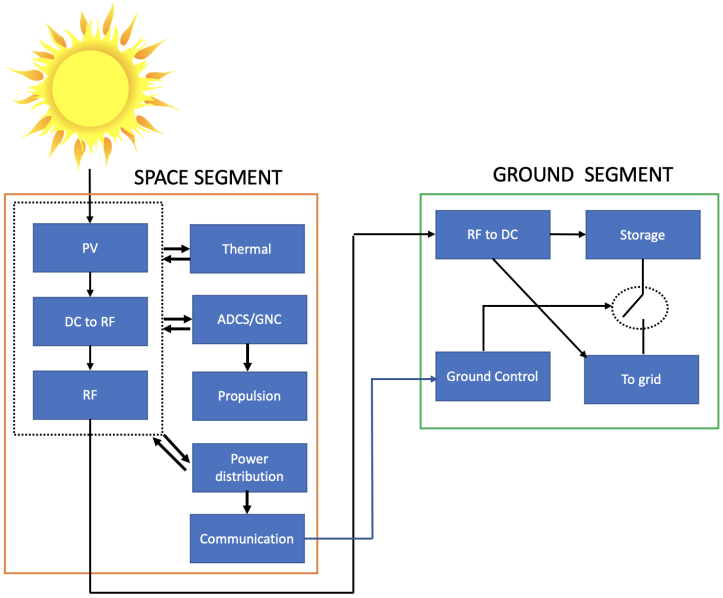

Figure 7: Block diagram describing the SPS

4.2 Slew Maneuvers

Slewing is an important aspect of our architecture since it can greatly influence the amount of power that effectively reaches Maui. The pointing requirements for collecting and transmitting power optimally are coupled, and it has been presented in [6] the most power optimal approach to slewing for a single-sided PV, single-sided RF (PV1RF1) architecture. The sun angle to maximize both collection and transmission at the same time is shown in Figure 8 below.

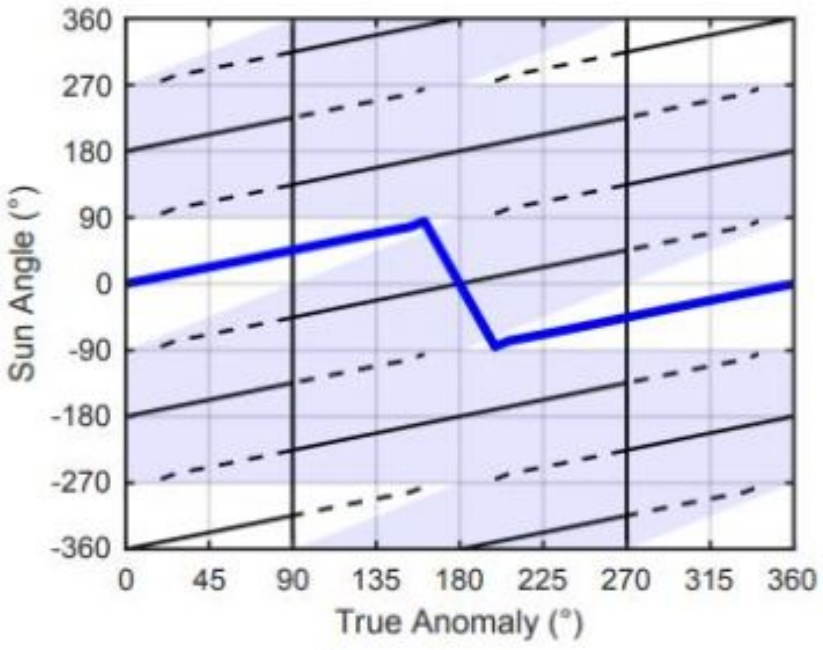

Figure 8: Optimal sun angle for PV1RF1 as a function of where the spacecraft is on its orbit [6]

The shaded blue areas show where the spacecraft can no longer satisfy the pointing requirements to transmit and collect power at the same time. During this section of the orbit, it is local midnight and the Earth is blocking the spacecraft from collecting any power. This is a perfect time for a slew maneuver, and the spacecraft must rotate by 180° in approximately 3 hours to satisfy pointing requirements once it reaches the other side of the orbit. The remainder of the orbit outside the gray

region shown in Figure 9 is one long continuous slew with optimal power guidance.

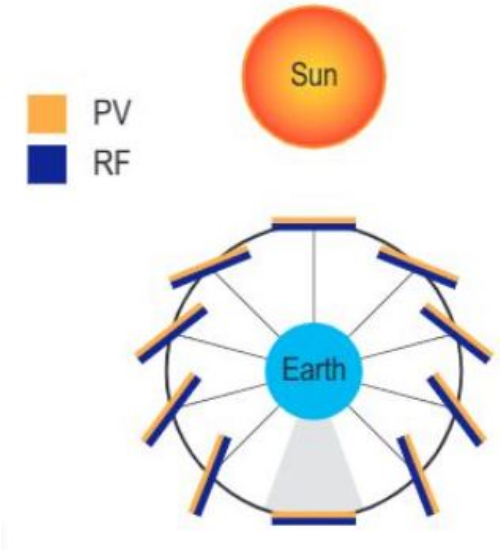

Figure 9: Power-optimal pointing for PV1RF1 [6]

4.3 Concept of Operations

4.3.1 Deployment and Initialization of Array

The 5 spacecraft will be launched in a powered off state prior to their initial deployment. Once they arrive to orbit, they will be released from their launch manifold and separate from the other spacecraft aboard the rocket. Once a spacecraft is far away enough from its neighbors, the startup mode will be commenced by kill switches. It is presumed that the spacecraft are properly configured for this task within the launch manifold prior to liftoff.

4.3.2 Startup Mode

The spacecraft's exposed solar panel surface provides the initial power required to be able to run the startup mode, as well as the onboard secondary battery that will be charged from the launch fairing. The spacecraft's first step is then to calibrate its ADCS sensors and then determine its orientation and location with relation to the sun, Earth, and stars. Following this calibration, the ADCS can be enabled, and the unit stabilized based off of the orientation data using its pulsed plasma thrusters. The spacecraft also enables its UHF transceivers to start communicating with the ground station and its neighbors.

4.3.3 Deployment Mode

Once the spacecraft is stabilized, it can begin its deployment sequence. This includes using the Xenon thrusters to perform an orbit transfer maneuver from GTO to GEO. Following its arrival, the spacecraft first deploys its booms, and then unfolds the remaining (and majority) of its photovoltaic surfaces that were not already exposed. It then uses the onboard thrusters to orientate itself towards sun so that it can receive maximum power, and charge the onboard secondary battery unit if necessary. It is assumed that the launch is organized such that there is no eclipsing issues before this point. The next step of the deployment mode is that the spacecraft sends signals to the ground station with the necessary telemetry for the ground station to verify the success of the deployment. Following this, the spacecraft uses the onboard thrusters to fully charge the CMGs in preparation of the slew maneuvers that will be necessary at later stages. Once the spacecraft has all of the energy necessary for nominal operation in the transmission mode, the spacecraft can begin to enable full communication and ranging with the rest of the constellation via its UHF transceivers and star sensors. Using the data from the

nearest spacecraft, the unit can adjust its position into a preprogrammed slot of the flying formation. Once it is within the desired location, it is reorientated appropriately towards ground RF target, and can begin to operate in the power transmission mode.

4.3.4 Power Transmission Mode

The main objective of the spacecraft is to provide power to the ground station, and hence the power transmission mode is its primary mode of operation. The solar array will collect solar radiation on the surface of the photovoltaics across the whole deployed area, and use the minimal amount of power for diagnostics, telemetry data transmission, and inter unit communication. The RF transmitters will be activated during this mode, and send power down towards the intended ground target. The inter unit communication and GPS receiver in the bus will ensure that this transmission is properly fixed and pointed. The spacecraft will perform the continuous 2 slews during the orbit when it reaches a high angle that makes its orientation relative to the sun too inefficient via the onboard CMGs and PPT. Following this, the CMGs will also desaturate for a short period via the pulsed plasma thrusts until the system detects that they are at the appropriate nominal level.

4.3.5 Safe Mode

If a component failure is detected, the RF transmission will cease immediately, and the spacecraft will enter safe mode. While in safe mode, telemetry will continue to send, and orbit maintenance will preside over slewing of any sort. The relatively critical station keeping tasks such as thermal balance and inter unit telecommunications systems will remain enabled. The spacecraft will await a ground station command to exit safe mode. The whole system reboots upon exiting safe mode, and it will also repeat the nondeployment steps of the startup and deployment mode sequences before resuming regular power transmission mode operations.

4.3.6 Decommissioning

At the end of the mission, or if the spacecraft sustains irreparable damage, or if it determines that it is unable to sustain full orbit, the spacecraft will enter a decommissioning mode. Upon entering this mode via ground station command from safe mode, the spacecraft will use its remaining resources to ascend to enter a GEO graveyard orbit at 300km, being careful to avoid any maneuvers that may interfere with other units.

5 Subsystems

5.1 Space Segment Subsystem Sizing and Power Requirements

The overwhelming majority of the mass of each individual spacecraft is the result of the mass of the PV and the transmitters. This yielded an estimate of 906.05 kg per spacecraft. Incorporating the rest of the spacecraft bus and components such as electronics, structure, ADCS, batteries, and propulsion will likely yield a final mass close to 906.05 kg per spacecraft based on preliminary components researched in 18.

5.2 Space segment

The space segment is a cluster of spacecraft flying together in a controlled manner. They will effectively form a flat structure. Each spacecraft consists of a central satellite bus serving as the hub for a modular sandwich structures[7] with PV on one side, RF on the other side, and a DC to RF converter in the middle. The flat plate structure is selected because one of the sides acts as a power collection mechanism and the other side acts as the power transmission medium. By using this architecture, most of the space segment geometry will be functionally active.

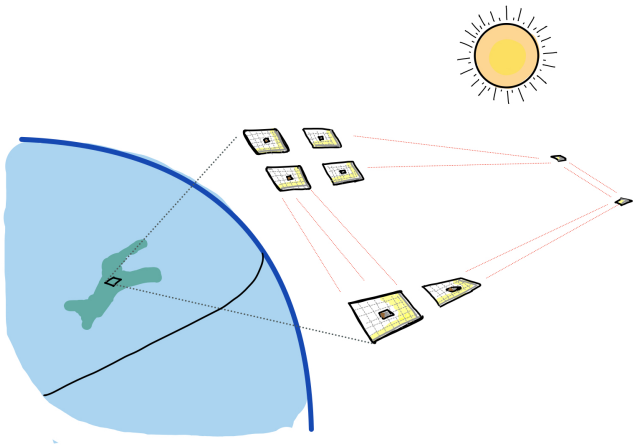

Figure 10: A schematic of the proposed architecture.

The converted power is affected by the efficiency of the photovoltaics(PV). PV has an efficiency of its own because of the Shockley–Queisser limit. There are other constraints as well, like reflections and tiny shadows from the metal wires that reduce the amount of sunlight accessing the solar cell. Thin Si cells are selected as a result of trade studies performed in Section-3.3.1.

The resulting power is then transmitted to Earth using phased arrays. The transmission frequency if selected to be 5 GHz. Each spacecraft will have these modules with a spacing of $\lambda/2 = 3$cm. This spacing is selected to ensure better main lobe characteristics.

Effectively, all the spacecrafts will align together to form a large flat plate in space. They will perform formation flying within safe distances, to collect sunlight through photovoltaics. A flat configuration is an effective solar energy collector because half of the plate acts as a collection mechanism and half acts as a transmission side.

5.3 Detailed Component Description Space System

The functional requirements of the SSPP system described within this proposal were used to determine the components that satisfy the operational goals of the SSPP. These operational goals have been outlined in the sections above, and are summarized as follows.

Satellite Bus: A CoTS GEOStar 2 Bus was chosen as an existing barebones structure for payload integration. This bus has a modular design capable of long term missions in GEO orbit, and includes a BAERad750 flight computer, power distribution module capable of sustaining 8000W, harnessing and interconnect, and payload integration. The bus supports electric propulsion and additional ADCS modules [32].

Payload: The primary payload of the SSPP Space Segment is the solar collection and transmission module each spacecraft contains and is designed around. This structure consists of a "sandwich" of PV solar collectors and RF transmitters embedded in a flexible substrate. A functional schematic is shown in Figure-11. The PV was chosen due to its long-term robustness to degradation in space, capable of maintaining a nearly consistent 20% power conversion efficiency over the course of a 20 year mission, as well as its less resource intensive design. A combination of these factors improves the feasibility of this choice, as it requires less raw material to produce Si based PV than GaAs based 3J or 4J PV. Additionally, this choice resulted in a lower overall number of spacecraft than a GaAs based PV technology. The flexible kapton RF patch antenna and chip scheme was chosen as it is technologically the simplest and most efficient method currently available, able to be folded efficiently, and something that can be manufactured easily in most modern facilities.

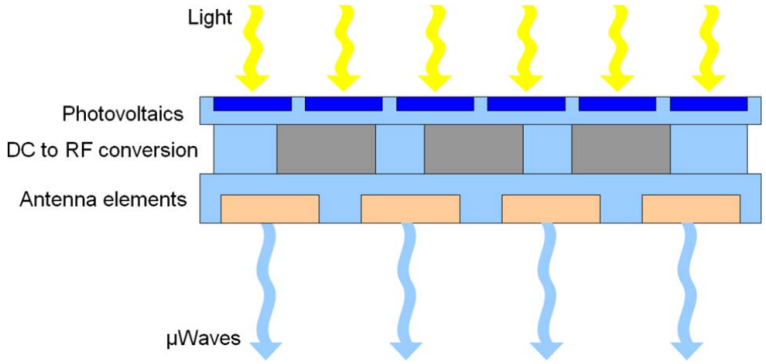

Figure 11: Functional layers in the sandwich module. [7]

Power: The spacecraft requires a centralized power source and distribution module, including the relevant harnessing and interconnect (H&I) that connects modules located on the primary spacecraft structure. These modules are included with the selected barebones CoTS GEOStar 2 bus chosen for payload integration. The Li-Ion spacecraft batteries are used by the spacecraft to store sufficient power (5kWh) for an eclipse, and are sized accordingly. The power distribution components are also sized analogously to GEO spacecraft of a similar mass profile.

Communications: The spacecraft will communicate with the ground station on a UHF transmitter. The chosen transmitter easily integrates with the spacecraft bus and will be nadir pointing during day-in-the-life (DITL) operations. This transmitter has a power draw of 1.4 W during DITL operations, and transmits at a frequency of 400-403 MHz.

ADCS & GNC: The strictest requirements for the space segment of the SSPP is the ADCS and GNC section. The satellites must maintain nadir pointing, achievable to sub 10mrad accuracy using a combination of reaction control moment gyroscopes (CMGs) and the spacecraft pulsed plasma thruster propulsion system. More importantly, the ADCS GNC system must maintain formation flying between several hundred spacecraft with a separation on the order of several meters. Prior studies have shown that using GNSS satellites from opposing sides of the Earth, it is possible to achieve a relative positional accuracy to 3 meter level accuracy using a "carrier phase differential relative positioning algorithm" [33] [34]. The satellites composing the space segment of the SSPP must maintain their relative positions with a resolution of centimeters, so additional methods must be employed to ensure power optimal formation flying. This will be done using a combination of UHF crosslinked rangefinding and optical bearing determination [34]. The simplest effective method of estimating spacecraft bearing optically is with a combination of light emitting markers on one spacecraft and a camera on another. Each spacecraft will thus have 4 sets of LED markers that will be optically tracked with a camera on a short extendable boom to determine the bearing of another spacecraft. During the initial approach to the incomplete formation, a spacecraft will be guided with a combination of UHF crosslinking and GNSS rangefinding. The position of an approaching spacecraft can be estimated with a high degree of accuracy. Upon reaching optically resolvable distances, the led markers will be tracked to determine the relative position between the formation and an approaching satellite. The satellite will unfold in place and assume its position within the formation. This process is repeated throughout the deployment and any subsequent supplement of satellites to the formation. The components were selected based on the necessary components for this GNC algorithm. During a daily eclipse, satellites may remain crosslinked to perform significant attitude maneuvers and maintain relative positioning.

Another important consideration related to ADCS is the spacing between each spacecraft for the formation flying. To transmit power effectively, all spacecraft must transmit power as a phased array. The optimal spacing for a phased array is $\lambda/2$, which corresponds to 3 cm for our transmission frequency of 5 GHz. However, spacing 60m x 60m spacecraft this close together would cause several issues, including concerns with collision risks. To determine losses from larger spacing, we performed MATLAB simulations on the percent energy from the main lobe obtained from various spacecraft spacing. In this simulation, each spacecraft was treated as a single source, and we used an array of

26 x 27 spacecraft to achieve our total of 692. Optimal spacing of $\lambda/2$ provides 84% main lobe energy from the phased array, which is a physical maximum value. It has been described in the literature that 3m of spacing can be achieved with GPS in GEO by using satellites from the other side of the planet [33]. This is a much more feasible spacing for the spacecraft, and the simulations show that the percent main lobe energy from this spacing is 80%, only a 4% decrease from optimal.

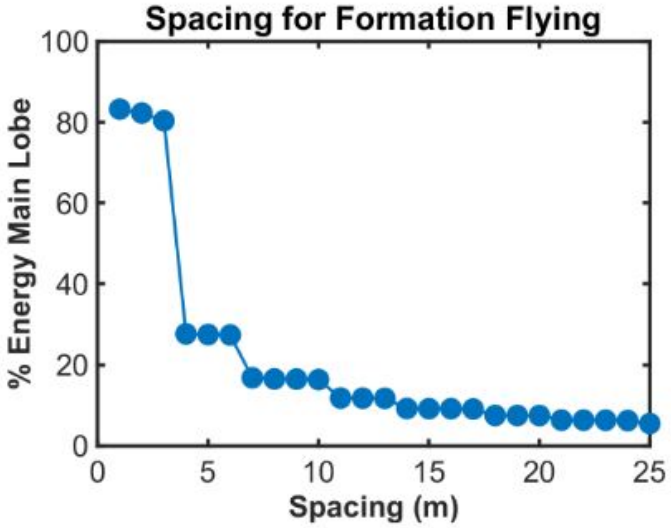

Figure 12: Percent main lobe energy as a function of phased array spacing

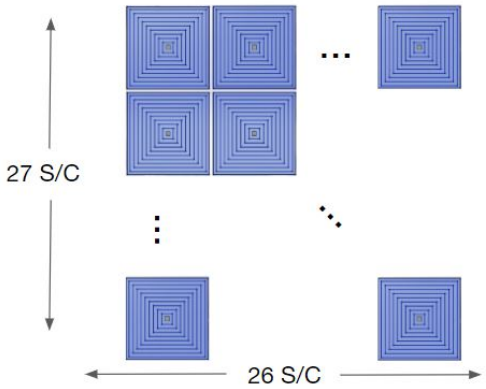

Figure 13: To-scale depiction of the 60m x 60m spacecraft with 3m spacing

Propulsion: The propulsion system for the spacecraft was sized based on similar GEO satellites [32]. Thus, a Xenon fueled ion thruster propulsion system was chosen for orbit raising from GTO to GEO. Electric propulsion was also chosen for standard maneuvering and positioning in formation flying due to the simplicity of the system and robustness to the space environment. The reference design for ion thrusters is based on the Dawn spacecraft, which utilized three of these thrusters [35]. A 906.05 kg spacecraft raising its orbit from GTO to GEO requires a delta-v budget of 1.954 km/s. The spacecraft will also have 4 pulsed plasma thrusters (PPTs) mounted at the end of each deployable boom, which will be used to aid the orbit raising maneuver and perform attitude control during DITL operations.

Structure & Mechanisms: The space segment consists of a large array of sandwich modules which need to be accommodated inside the launch vehicle assembly. We select the Caltech's ultralight packaging and deployment concept[8] which has been demonstrated in 2019 with a scaled down version of 1.9x1.9m. This is proposed to be scalable to 60x60m. A schematic of the deployed configuration is shown in Figure-14. This will encompass multiple repeating rectangular and triangular modules.

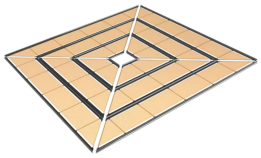

Figure 14: Power collection structure in deployed state.(Only three square strips are shown)[8]

The deployment mechanism consists of a central hub of 4 cylinders between which the structures are wrapped. This includes thin polyimide membrane on which the photovoltaics and transmission antennas are embedded. The unfolding is achieved with the help of elastic energy release from the strips. The final structure is stiffened with the help of longerons and battens. A brief idea of the packaging is shown in Figure-15.

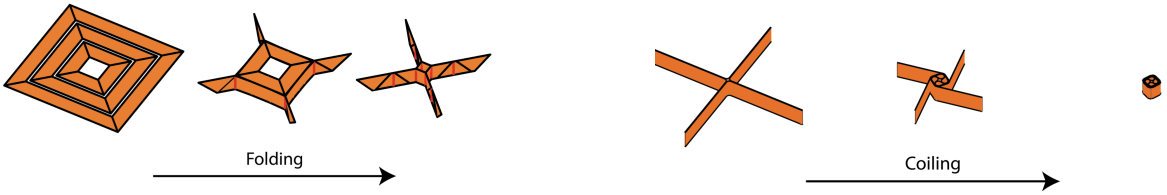

Figure 15: Packaging of the space structure.[8]

The prototype demonstrated[8] has a size of 1.7 x 1.7 m, with diameter of each cylinder as 63.5mm and 4 such cylinders in the core. When placed together, they form an effective circle of diameter 179mm. The stowed diameter of the structure is 185mm as reported[8] with a safety coiling factor of 2.5. As seen in Figure-15, after end of folding, we get four ends of folded ends which account for thickness of 3 strips for the prototype. An approximation of scaled up structure is done with similar idea but 30 strips total with a spacing of 1 m between consecutive strips as shown in Figure-16. Now each of the four ends after folding will have a thickness of 30 strips. The scaled up configuration will have diameter of 100mm and a height of 1m. This will change the effective core diameter from 179mm to 282mm. All this information is used to estimated the stowed diameter of 1.58m based on 50µm strip thickness and 2.5 safety factor for coiling.

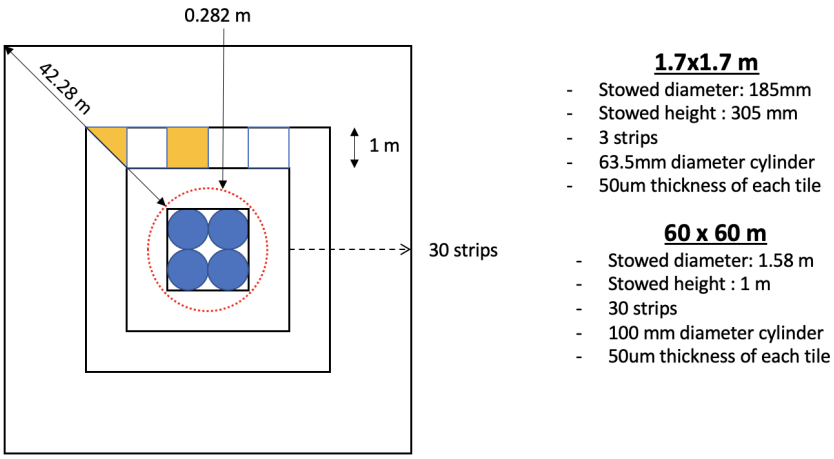

Figure 16: Scaling of the 1.7m x 1.7m mechanism to 60m x 60m mechanism.

The spacecraft is of size 1.75 x 1.7 x 2.8m as per the bus selection and the stowed dimensions of the mechanism. We plan to include five satellites in one launch vehicle based on launch volume constraints as shown in Figure-17.

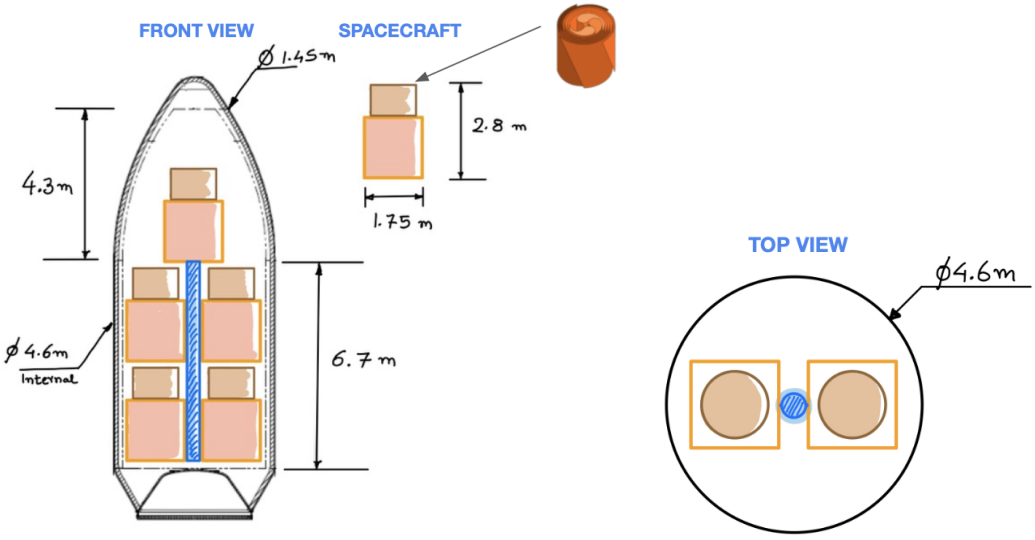

Figure 17: Spacecraft integration with Falcon-9

Thermal Control: Thermal control of the spacecraft will be a combination of passive and active control schemes. Multi Layer Insulation (MLI) will be used to cover sensitive instruments to isolate them from heat. This will be done with a high absorption and low emissivity MLI. Since one side of the spacecraft i.e. the power collection side, will be regularly facing the sun, it will tend to absorb more heat during the mission life. To appropriately distribute the heat energy, heat pipes will be used which will move heat from hot side of the spacecraft to the cold side. To reinforce this motion, we will include a few heaters on critical components within the bus to ensure optimal operational temperature. The cooler side or the transmitting side of the spacecraft will have radiators incorporated which will reject heat into deep space.

Photovoltaics As detailed in Section-3.3.1, 40 µm flexible Silicon cells are decided as photovoltaics for power collection. Each cell has a size of 40mm x 40mm and weighs 0.08 mg.

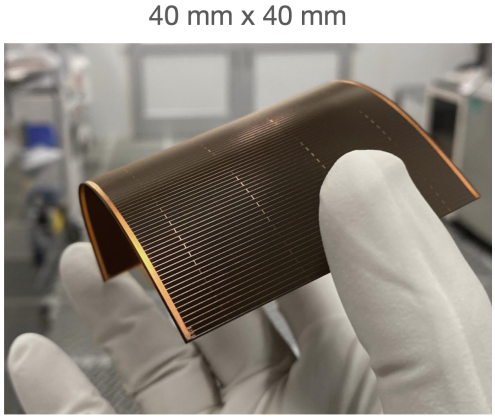

Figure 18: Thin Silicon solar cell from Solestial.[4]

5.3.1 DC to RF Chip and Phasing Chip

In order to convert the power absorbed by the PV, we will be using a custom DC to RF chip and a custom chip specifically for phasing our arrays. The phasing chip is already available at Caltech, and these can both be manufactured onto the RF patch antenna described below quite trivially. These chips should weigh on the order of a few fractions of a gram each, and are about a square centimeter per individual patch antenna with a thickness of less than 1mm. The total cost for the development of each is insignificant when compared to their manufacturing due to them being relatively normal electronic components, even when taking into account the requirement for them to be space hardened,

and as such their estimated value is taken into account by the 2 million dollar value of the RF patch antenna PCBs. The DC to RF conversion is about 60 percent efficient.

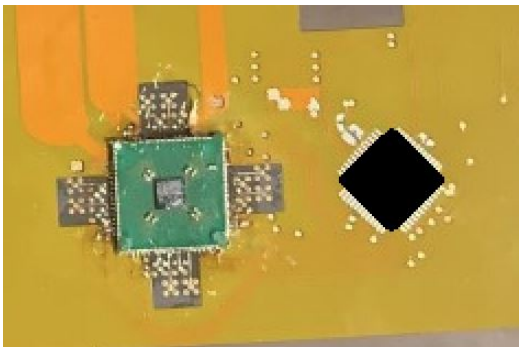

Figure 19: Phasing and DC to RF Chips in current Prototype

5.3.2 RF Patch Antenna

The RF patch antennas serve to transmit the power converted to RF to the ground array. They come in 4 x 4 units spaced at $\lambda/2$ apart. Thus each unit is 75x75 square mm, and have been empirically estimated to have a weight of 5 grams per unit. However, we can further reduce this weight to about that of kapton, the thinnest of which is 13 um and has a weight of 1.42 g/cc, for a total weight of 127.8 kg per space craft [36][37]. This type of patch antenna design is very common, and does not need a development cost, and can be easily manufactured by any flexible PCB company. As stated above, an estimated order from PCBgogo [38] puts the total cost at about 2 million dollars per spacecraft.

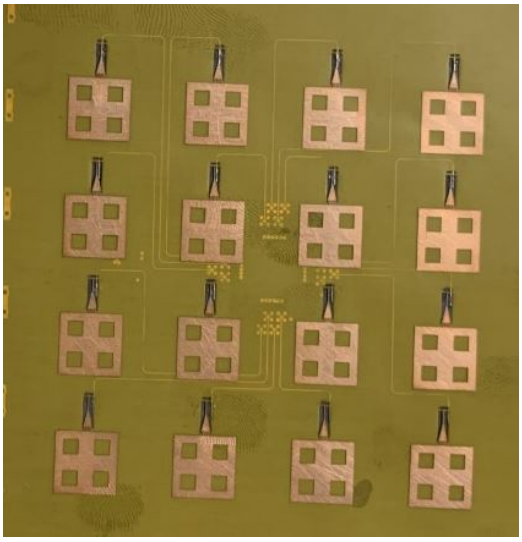

Figure 20: RF Patch Antenna on Kapton

5.3.3 Power Distribution

Our spacecraft bus comes equipped with an innate power distribution system capable of 8000 W of power draw, and thus this is accounted for in the cost and weight estimates of the bus. The primary point of this component is to convert the electricity going to our bus from the battery or nearby solar panels into a useable voltage for the components, such as the CMGs, ADCS, sensors, transceivers, etc.

5.3.4 Batteries

We calculated it would take about 4.8 kWh of battery storage to ensure that our spacecraft bus can continue to operate all components in the longest possible eclipse time of 72 minutes. Thus, we need about 5kWh to account for any dissipative losses. Projecting the current price for lithium ion

batteries, this amounts to a cost of 5000 dollars around 2030, and using the Eagle Picher spacecell 30 Ah, we will need about 50 kg of batteries to do so. These batteries will continue to be charged when not eclipsed after their initial charge from the launch fairing. [39] [40]

5.3.5 UHF Transceiver to Earth

We require a method to send our telemetry data to Earth. To accomplish this, we plan to use the UHF Transceiver II that is made by Endurosat, has plenty of flight hardening, and is relatively lightweight. It costs $5,500, weighs 94g, and uses 1.4 W [9].

Figure 21: UHF Transceiver for Telecom with Earth and Interlink [9]

5.3.6 UHF Transceiver Interlink

For the constellation to be able to effectively formation fly, it needs to be able to be able to communicate with its sub units. This can be easily accomplished by a second UHF transmitter that is identical to the one above [9]. This also adds in a level of redundancy in that if either one fails, the other transceiver can be used to send telemetry to Earth or the constellation.

5.3.7 CMGs

Airbus 15-45S 3-Axis CMGs are being used to perform attitude stabilization and assist with slew maneuvers during DITL operations. A 1000kg spacecraft equipped with 4 CMGs is capable of slewing at 3°/s. These CMGs will be used for attitude control during orbit raising and detumble, as well as DITL slew maneuvers. The mass and power characteristics are included in Table 8 and Table 9

5.3.8 Star and Sun Sensors

We are planning to help our structure orientate itself via both sun and star trackers. We will be using the NSS Cubesat Sun Sensor since it should be decent enough for just sun pointing. It costs 3300 dollars, weighs under 5g, and uses less than 50 mW. Our star tracker will be a bit higher grade, as we need to accurately position our spacecraft especially within the eclipse to avoid collisions, as well as organize our formation flying by using the tracker to observe the LEDs from local satellites. The ST-16RT2 from Rocket Labs has great flight heritage for being relatively modern, weighs 158g, costs $120,000, and takes only 1 watt to run.

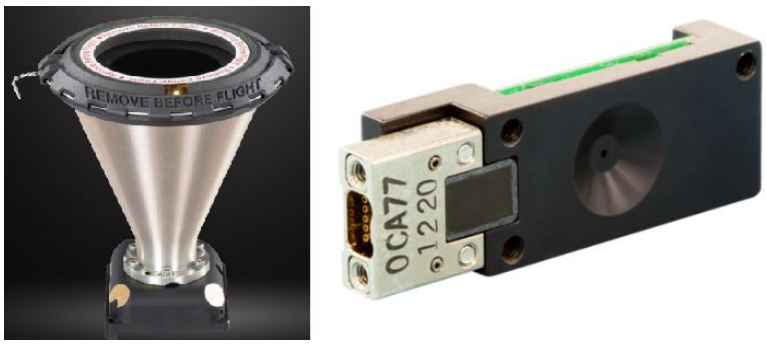

Figure 22: Star Sensor (left) [10] and Sun Sensor (right) [11]

5.3.9 LED Markers

The spacecraft requires LED markers on its bus and ends in order to be able to be detected by other spacecrafts' star sensors and orientated accordingly to prevent collisions. Since this is a simple electronic component with only a few instances, the cost, weight, and mass are negligible even when space hardened.

5.3.10 Pulsed Plasma Thrusters

Our spacecraft will utilize 4 pulsed plasma thrusters, each located on the end of the 4 diagonal booms for maximal stabilization torque. These thrusters will be similar to the ADD SIMP-LEX mission, also draw on heritage from the EO-1 mission, and produce .1 N of thrust each. This is enough to slew our spacecraft at a rate that is four times that of the CMGs, meaning that we can easily safely maneuver our spacecraft and recharge the CMGs concurrently. Each thruster weighs 20 kg including fuel at BOL, can operate for over 10,000 hours, and requires 80 W. The total cost for all four thrusters is 100,000 dollars. [41]

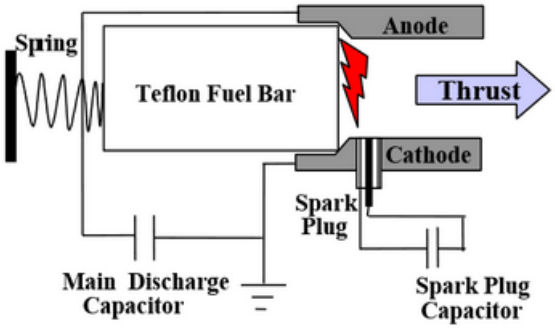

Figure 23: Pulsed plasma thruster diagram

5.4 Xenon Ion Thrusters

Performing an orbit raising maneuver to transfer from the GTO orbit where the launch vehicle releases the satellites to GEO orbit requires more powerful thrusters than the pulsed plasma maneuvering thrusters outlined in section 5.3.10. The thrusters chosen for this purpose are capable of delivering 91mN of thrust at an ISP of 3100s. A 906.05kg spacecraft performing GTO to GEO orbit raising maneuvers requires 55kg of xenon propellant to deliver 1.954Km/s of delta-v to raise its orbit. Each SSPP satellite carries two xenon thrusters for redundancy, and a total of 55kg of propellant (supplemented by the PPT) for orbit raising.

5.4.1 Thermal Management

To ensure all of our electronics in the bus are at a functional temperature, we can use a polyimide thermofoil heater. These each are about 2 grams, and thus have a negligible weight and cost. They

require 3.7 W, so assuming that we need 3-4 per bus, we can attribute a necessity of about 12 W for heating in the eclipse period to keep our electronics functional[12]. We assume that the rest of the spacecraft is made in a fashion that lets the solar panels and RF sections operate nominally in the temperatures that the spacecraft encounters.

Figure 24: Polyimide Thermofoil heater for ensuring electronics are operational in the bus [12]

Spacecraft Mass Budget						
Subsystem	**Component**	**Name**	**Vendor**	**Quantity**	**Mass Each [kg]**	**Mass Total [kg]**
Payload	PV	Solestial 20um	Solestial	2.25E+06	8.00E-05	180
	Transmitter + DC-RF IC	N/A	N/A	6.40E+05	2.00E-04	127.8
Power	Spacecraft Battery	Spacecell 30 Ah	Eaglepicher	50	1	50
Communications	UHF Transciever	UHF Transceiver II	Endurosat	1	0.094	0.094
	Flight Processor	BAE RAD750	Northrop (inc. w/ bus)	1	N/A	N/A
	Command and Data Handling	MIL-STD-1553, CCSDS	Northrop (inc. w/ bus)	1	N/A	N/A
ADCS & GNC	CMG	Avionics 15-45S	Airbus	4	18.4	73.6
	Star Sensors	ST-16RT2	Rocket Labs	1	0.158	0.158
	LED Markers	N/A	N/A	10	N/A	N/A
	UHF Transciever	UHF Transceiver II	Endurosat	1	0.094	0.094
	Sun Sensors	N/A	NSS Cubesat	1	0.005	0.005
	GPS Reciever	Sentinel M-Code	General Dynamics	1	2.5	2.5
Propulsion	Pulsed Plasma Thruster	N/A	EO-1/ADD SIMP LEX ref.	4	20	80
	Xenon SEP	N/A	DS-1 ref.	2	18.4	36.8
	Fuel (Xenon SEP) (EACH)	N/A	N/A	1	55	55
Structure	Spacecraft Structure + Booms and Mechanisms	GEOStar 2 Barebones	Northrop / Orbital ATK	1	N/A	300
Thermal	Thermal Heater	Polyimide Thermofoil Heater	Minco	3	0.002	0.006
					Total Mass:	906.057

Table 8: Spacecraft Mass Budget

Spacecraft Power Budget						
Subsystem	**Component**	**Name**	**Vendor**	**Quantity**	**Power [W]**	**Power Total [W]**
Payload	PV	Solestial 20um	Solestial	2.25E+06	N/A	N/A
	Transmitter + DC-RF IC	N/A	N/A	6.40E+05	N/A	N/A
Power	Spacecraft Battery	Spacecell 30 Ah	Eaglepicher	50	2.5 to charge	125 to charge
Communications	UHF Transciever	UHF Transceiver II	Endurosat	1	1.4	1.4
	Flight Processor	BAE RAD750	Northrop (inc. w/ bus)	1	N/A	N/A
	Command and Data Handling	MIL-STD-1553, CCSDS	Northrop (inc. w/ bus)	1	N/A	N/A
ADCS & GNC	CMG	Avionics 15-45S	Airbus	4	25	100
	Star Sensors	ST-16RT2	Rocket Labs	1	1	1
	LED Markers	N/A	N/A	10	0.25	2.5
	UHF Transciever	UHF Transceiver II	Endurosat	1	1.4	1.4
	Sun Sensors	N/A	NSS Cubesat	1	0.05	0.05
	GPS Reciever	Sentinel M-Code	General Dynamics	1	8	8
Propulsion	Pulsed Plasma Thruster	N/A	EO-1/ADD SIMP LEX ref.	4	80	320
	Xenon SEP	N/A	DS-1 ref.	2	2300	4600
	Fuel (Xenon SEP) (EACH)	N/A	N/A	1	N/A	N/A
Structure	Spacecraft Structure + Booms and Mechanisms	GEOStar 2 Barebones	Northrop / Orbital ATK	1	8000W capacity	N/A
Thermal	Thermal Heater	Polyimide Thermofoil Heater	Minco	3	4	12
					Total Power:	5,046.35

Table 9: Spacecraft Power Budget

5.5 Bus

Producing hundreds of satellites requires a robust production line capable of delivering far more satellites to GEO than a typical scientific mission meriting a ground-up design for the spacecraft bus. For this reason, instead of designing a spacecraft bus from scratch, the Northrop Grumman DS-44a GEOStar-2 Satellite bus was chosen as the carrier for the SSPS payload. This satellite bus integrates all components necessary to operate in a GEO orbit and successfully deploy the sandwich structure that collects and transmits power on orbit. The bus integrates support for up to 1000kg payloads, 8000W power, 36VDC, Li-Ion batteries, 3-Axis ADCS zero momentum ADCS solutions, electric propulsion modules, uses MIL-STD 1553B, CCSDS command and data handling protocols, and includes a radiation hardened BAE RAD750 flight processor at the core of the avionics subsystem [32].

Figure 25: GEOStar 2 Core Bus

5.6 Launch segment

The launch segment of the proposed architecture consists of launch vehicle integration and testing, launch operations, and satellite release operations. Launch vehicle integration includes attachment of five spacecraft to the deployment and integration structure inside the payload fairing. Upon successful launch vehicle integration, each grouping of five spacecraft is subjected to launch vehicle integration testing, which includes pre-release standby power and communication modes. The launch vehicle satellite integration structure allows for 5 SSP spacecraft to be stacked within the Falcon 9 payload fairing, and provides the necessary hold down and release mechanisms that facilitate safe satellite release upon launch vehicle arrival to GTO. The launch vehicle is volume limited.

5.7 Ground segment

The ground segment of the proposed architecture consists of a rectenna farm, energy back-up storage, and ground facilities/maintenance. The rectenna farm has 8.99 km^2 of rectenna area with each antennae spaced 3 cm apart, which corresponds to a distance of $\lambda/2$. Power collected from these antennae pass through the ground station architecture to service Maui. Tesla Megapack [13] lithium ion batteries will be used for utility energy storage on the ground.

Figure 26: Tesla Megapack modular batteries [13]

Required Power (MW)	100
Noneclipse Power (MW)	100.98
Power to Battery (MW)	0.98
Required Eclipse Energy (J)	1.48E13
Energy Transferred for Eclipse (J)	1.52E13

Table 10: Power transmission calculations incorporating eclipse time

To ensure that 100 MW is being supplied to Maui continuously, we need to account for eclipses and size ground station batteries for storing extra energy transmitted during non-eclipse. A conservative estimate for eclipse times is 41 hours, since there are two 41 hour blocks of eclipse time centered around the equinoxes with the longest continuous eclipse amounting to about 3 hours. This battery oversizing is to ensure that the battery has back-up power if any two eclipse times are close to being back-to-back.

By storing 0.98 MW of effective power during non-eclipse times, there is more than enough energy stored to provide 100 MW of power for up to a 41 hour eclipse. Required eclipse energy was calculated by calculating 100 MW over 41 hours. Energy transferred for eclipse was calculated by using 0.98 MW over half a year minus 41 hours (total noneclipse time with overhead).

The Tesla Megapack is readily available and can be scaled infinitely. It stores energy on the order of MWh, and for the required eclipse energy, we would need 1,178 units of batteries.

Figure 27 displays the power flowdown for our architecture, from space to ground. On-orbit, 3.39 GW is collected, which becomes 139.4 MW after space conversion inefficiencies, including DC to RF. After ground conversion inefficiencies including RF-DC, inversion, and DC-AC, this becomes on average 101.2 MW. After storage efficiencies of 0.9 for charging and discharging, the effective power stored in batteries is 0.98 MW.

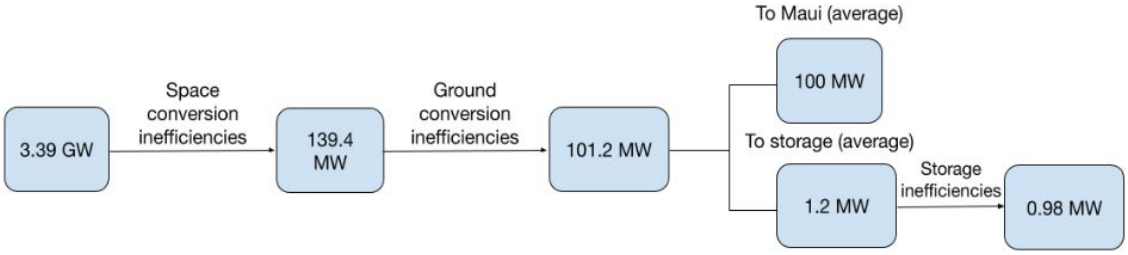

Figure 27: Power flowdown to ground segment displaying inefficiencies.

6 Power analysis

6.1 Received and transmitted power (Space segment)

The overall system efficiency in the space segment can be decomposed into several subsystem efficiencies namely Photovoltaics unit(PV), DC power to RF power conversion unit(DCRF), Patch array antenna unit(Tx) and sun inclination angle effective(Geometric).

PV efficiency BOL(Sec-3.3.1)	η_{PVb}	0.218
PV efficiency EOL	η_{PVe}	0.196
DC-RF efficiency[7]	η_{DCRF}	0.6
Antenna efficiency[7]	η_{Tx}	0.95
Geometric efficiency[18]	η_{geom}	0.5

Table 11: Efficiencies for Space segment

The PV efficiency at EOL provided in Table-11 comes from specifications given by vendor website[4].

Assuming an area of 60x60 m^2 per spacecraft based on packaging scheme, the power incident and emitted from each spacecraft are shown in Table-14. Grid power can be related to the subsystem efficiencies using equation-1

$$P_g = \eta_{PV}\eta_{DCRF}\eta_{Tx}\eta_{\text{geom}}\ \eta_{\text{dif}}\ \eta_{RFDC}\eta_{DCAC}\left(\frac{f}{cr}\right)^2 A_{Tx}A_{Rx}\left\{(AM0)A_{PV}\right\} \tag{1}$$

Where,
P_g = grid power
f = frequency of transmission
r = range of travel or distance between receiver and transmitter
c = speed of light
η_i = efficiency of subsystem "i"
A_{Tx} = area of transmitter
A_{Rx} = area of receiver
A_{PV} = area of Photovoltaics

For flat space power collection design, it can be assumed that the A_{PV}=A_{Tx} to ensure maximum geometric efficiency. Area of transmitter can be related to the area of receiver using equation-2. Number of rectifiers can be calculated using equation-3.

$$A_{Rx} = 1.488\pi\frac{(rc)^2}{f^2 A_{Tx}} \tag{2}$$

$$N_{rec} = 4\left(1.488\pi\frac{r^2}{A_{Tx}}\right) \tag{3}$$

Input	Notation	Value	Units
Lattitude	Phi	20	deg
Sun Solar intensity	AMO	1366	W/m2
RF frequency	f	5.00E+09	Hz
Speed of light	c	3.00E+08	m/s
Distance bw Tx and Rx	r	3.65E+04	km
Grid Power	Pg	1.00E+08	W

Table 12: Inputs for power calculation

Since Maui is located at 20^oN , the range won't be exactly the altitude of the orbit. This is because the subsatellite point of the GEO spacecraft is at the equator. As a result of orbital trade studies and transmission frequency trade, a list of inputs are used to calculate power losses on orbit.(Table-12)

Entity	Symbol	Value	Units
Area of PV	A_{PV}	2.49	km^2
Area of transmitting array	A_{Tx}	2.49	km^2
Area of rectenna array	A_{Rx}	8.99	km^2
Number of rectannas	N_{rec}	2.76E+09	

Table 13: Outputs for the entire fleet of spacecrafts

Location	Power
Power incident on PV (MW)	4.92
Power sent from S/C to earth(kW)	275.74

Table 14: Power figure for each spacecraft.

The results from the power calculations are shown in Table-13. Power values for each spacecraft are given in Table-14 Detailed values are given in Appendix-**??**

6.2 Collected power and available on ground(Ground segment)

The ground segment is considered to be a field of rectifier antennas with a large power storage area to compensate for eclipse times of 41 hours twice per year. This is because spacecrafts in GEO are susceptible to shadowing from earth during vernal and autumnal equinoxes. Since the RF transmission has only limited directivity, its mandatory that we account the energy for the main lobe alone. The parameters affecting the ground segment power are - amount of energy encapsulated in the main lobe, rectenna efficiency for conversion of the received RF waves to DC power and finally inefficiency of converting DC power to AC. This is all shown in Table 15.

% Energy in main lobe	η_{dif}	0.8
Rectenna efficiency RF in, to DC out	η_{RFDC}	0.82
Battery efficiency	η_{DCAC}	0.81

Table 15: Efficiencies for Ground segment

To convert RF signals to DC, a rectifier antenna will be used. A dipole type plane polarized rectenna(Figure-28) is chosen because of the higher demonstrated[42] efficiency and working frequency(5.8 GHz) with antenna impedance matched to rectifier. It will have following components:

- RF capacitor short chip

- Schottky diode
- Dipole antenna
- Low pass filter with capacitor strips
- Substrate

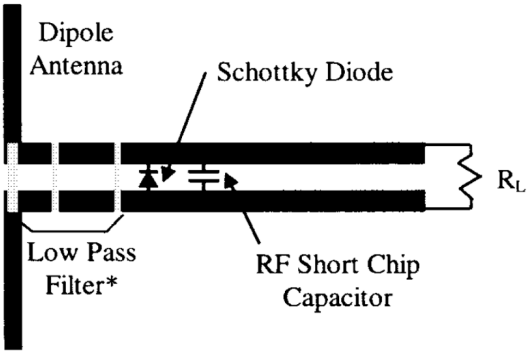

Figure 28: 5.8-GHz rectenna element.

6.3 Required utility storage on ground

A back-up storage system is required to provide 100 MW continuously on Maui when solar power is not being transmitted. The Tesla Megapack is a promising energy storage choice and will be used for the ground segment. These lithium ion batteries are capable of each storing power on the order of MWh, are infinitely scalable, and are readily available to purchase now. Given the energy transmitted in Table - 10 , a total of 4,222.23 MWh is necessary. A total of 1,178 units will be required, which will cost a total of **1,812M$** including installation.

7 Cost Estimates

7.1 Photovoltaics

Initial costs per m^2 are estimated using available literature[21] as provided in Table-4. These numbers are based on studies done in 2000. Hence an inflation adjustment is done to year 2022 and a learning curve data was used till 2015 and the costs were assumed to be invariant of learning after that.

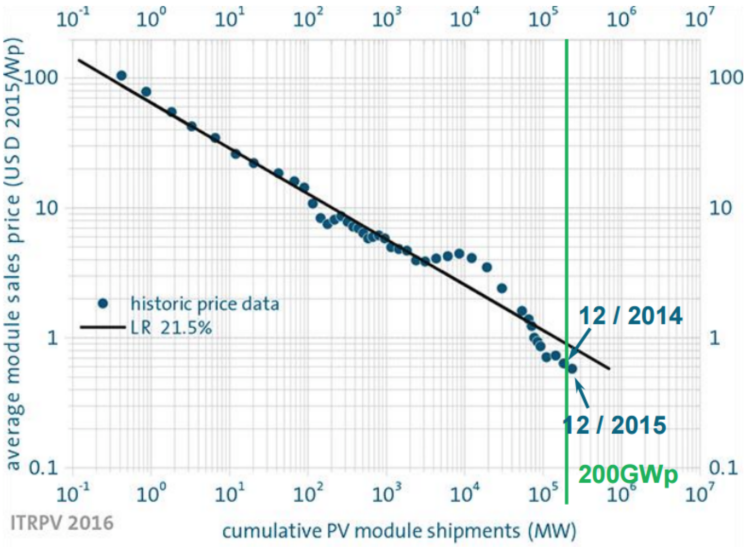

Figure 29: This graph shows a learning factor of 21.5% from 1976 through 2015. Short-term fluctuations are partly due to supply chain issues. Source: International Technology Roadmap for Photovoltaic[14]

It is assumed the cost of thicker Silicon cells will be similar to ultra thin Silicon cells. And hence from Figure-30, it can be estimated that the cost of solar panels decreased from around 10$/W to 0.61$/W from year 2000 to 2015. This brings down the cost of 20µm Si cells from 22.5 k$/$m^2$ to 1.3 k$/$m^2$. Full constellation on orbit requires a total PV of **3.41 B$**.

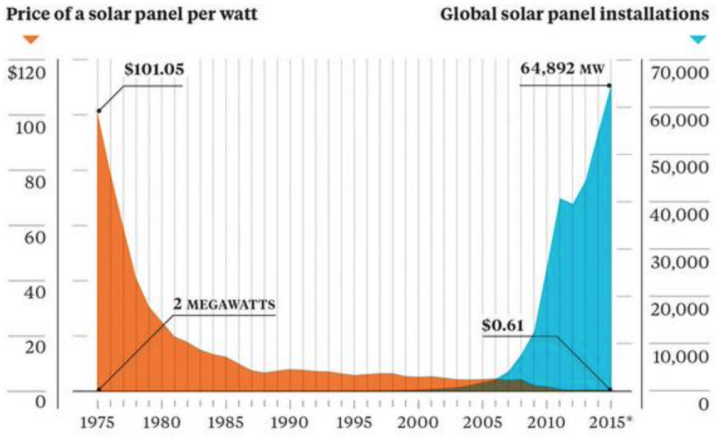

Figure 30: Solar panel costs and global installations from 1975 to 2015.
Source: Earth Policy Institute/Bloomberg.

7.2 DC to RF and Patch Antennas for Transmitters

The patch antenna transmitters along with their DC to RF chips can be roughly estimated from a material and assembly cost via manufacturer orders. For the required 640,000 units, the PCBgogo calculator yields a cost of about 2 million dollars per spacecraft, or a total of 1.38 billion dollars for the whole array [38].

7.3 Rectennas

Estimation of cost of each rectenna is done on the basis of the components as shown in Table-16. Overall cost of each rectenna is estimated to be 9.36$. Total number of rectennas required are 2,628,143,510 from equation-3 which amounts to **24,607M$**. For an over all area of 9.45 km^2, the cost per m^2 of area for rectennas comes out to be **2,603 $/m^2**

Entity	Cost($)	Quantity
RF capacitor short chip	2.6	1
Schottky diode	0.633	1
Dipole antenna	4.0	1
Low pass filter with capacitive strips	0.22	1
Substrate	1.91	1
TOTAL	9.36	

Table 16: Rectenna cost based on individual components

This method yields a cost of 2880\$/m^2 which is far more than the proposed ground segment cost by Caltech's cost estimate which is 210\$/m^2. So for estimation of LCOE, we use the Caltech's estimate as rectenna cost per square meter.

7.4 Labor

Labor cost is calculated based on a sample estimation problem in Appendix-C in the NASA Cost estimation handbook[43]. The cost estimating relationship is assumed to be the mass of the payload i.e. the photovoltaics and the phased arrays.

Per satellite labor estimate		
Cost Estimating relationship(CER)	25	hours/kg
Mass of PV+RF	307.8	kg
Direct labor hours	7695	hrs
Labor cost	80	\$/hr
Direct labor costs	6.16E-01	M\$

Table 17: Labor cost estimation

7.5 Summary

Space segment	
Subsystems	**Total Cost (M$)**
Photovoltaics	3,410
Power Transmitter	1,384
Bus Components	398.66
Production Facilities	100
Labor(Assembly)	425.9
Total	**5,719**

Table 18: Space segment costs

Ground segment	
Component	**Total Cost (M$)**
Rectennas	1,890
Energy storage	1,812
Land Cost	16.85
Facilities Dev.	207.6
GS Maintenance	581
Total	**4,507**

Table 19: Ground segment costs

Launch segment	
Subsystems	**Total Cost (M$)**
Launcher	8,304

Table 20: Launch segment costs

Space segment		
Subsystem	**Component**	**Total Cost (M$)**
Payload (Sandwich Module)	PV	4.94
	DC-RF	0 (included in transmitter)
	Transmitter	2
Power	PDB	.01
	Battery	.0048
Communications	UHF Transceiver	.0055
ADCS & GNC	Avionics / Flight Computer	.006
	3-Axis CMG	.2
	Star Sensor	.120
	LED Markers	.001
	UHF Transceiver for crosslinking	.0055
	Sun Sensor	.0033
Propulsion	PPTs (x4)	.1
Structure	Deployable Booms	.07
	Spacecraft Structure	.05
Thermal Control	Structure and Sandwich Design	N/A
Total per S/C		7.5161
Grand Total (All Spacecraft)		5201

Table 21: Cost of individual components per Spacecraft.

All the costs put together yield an Levelized Cost of Electricity(LCOE) of 1.06 $/kWHr.

8 Risk Mitigation

There are a lot of risks associated with large spacecraft in general, and we try to mitigate several of them in our design. The first risk that we address is spacecraft collisions. During the initial deployment phase, we minimize collision risks by having the spacecraft spread out, and then unfold relatively far away from each other before joining the constellation. Inter spacecraft collisions are further avoided during power transmission mode via the redundancy of using GPS, UHF inter spacecraft telecommunications, and optical sensing from LEDs and star/sun sensors to help establish positions

confidently. These communications can be designed around a safety critical control scheme in order to further ensure operational efficacy. Our spacecraft are also adequately spaced as per the literature precision, which has argued that a 3m positional separation formation flying is possible with GPS in GEO. [33] [34]

Another risk that we address is the potential for collisions from malfunctioning spacecraft by implementing a decommissioning procedure to prevent damaged spacecraft from "clogging" up the array and damaging both the power lobe profile and increasing chances that a collision occurs. When a spacecraft has such an issue, we also have the safe mode planned so that the RF transmission is disabled to ensure that no misdirected phasing or power is directed at nonintended targets.

Our spacecraft is also controlled via both four CMGs and four PPTs in combination to ensure the stability of the system. Having multiple PPTs per spacecraft helps to ensure better balance, control, and redundancy in our maneuvers, and also means that we will have the ability to reposition our spacecraft in most catastrophic scenarios. These thrusters and CMGs are also part of the large number of heritage components in our system. This includes most components outside of the RF transmitters and composite booms, for which we can perform rigorous ground testing to verify space hardening.

9 Timeline

The Space solar power mission is stretched to about 9 years of preparation from 2021 end to 2029. The first technology demonstration is planned in year 2025 when the design has matured enough and a part of ground station is operational. With this being done, it will be enough to establish the power transmission efficiencies with the tech demo. The first fleet of 116 spacecrafts are to be ready before 2030 and will be launched in first half 2030. Simultaneously, the second fleet will undergo the final test and and will be ready for launch in the second half of 2030 and so on. The architecture will be complete by the end of year 2032 and will be operational till 2053.

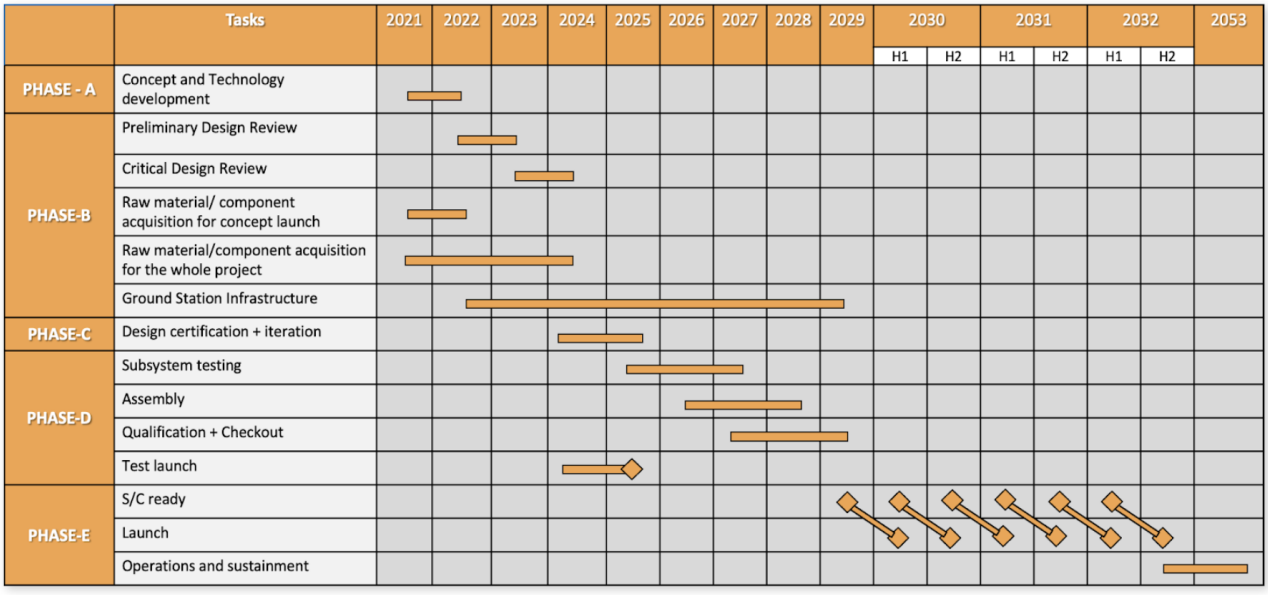

Figure 31: Timeline for the overall mission

10 Comparison to Baseline

This section will have a quantitative comparison between the Caltech Baseline SSPP and the SSPP Architecture proposed here in the final draft. Qualitatively, this proposed architecture resembles the Caltech Baseline, with key differences in trades made with the intent to demonstrate manufacturability and feasibility by 2030. Both architectures use a planar, single sided PV architecture in GEO with

a nearly constant PV efficiency of 20%. Each spacecraft module for both systems are 60 m x 60 m. Caltech SSPP has a slightly higher number of spacecraft, which is 792 as opposed to the Proposed SSPP of 692. Both architectures use Falcon 9 for at least one of the LCOE estimates. Formation flying is a central aspect of both designs, but the spacing for the Proposed SSPP is 3 m, while for Caltech, it is claimed to be at optimal spacing of $\lambda/2$. The transmission frequency for Caltech is at 10 GHz, but 5 GHz is used for the Proposed SSPP to take advantage of its higher efficiencies. This leads to a significant difference between the ground station areas for the two architectures. Caltech's rectenna area is 0.47 km^2, while Proposed SSPP has a ground area of 8.99 km^2 due to not taking advantage of some optical effects. The end-to-end efficiencies are quite similar (2.57% and 2.97% for Caltech and Proposed, respectively), and the main differences derive from slightly higher assumed transmitter frequencies in the Proposed architecture. Stemming from these efficiency differences, Caltech is producing 3.9 GW on-orbit, while the Proposed design produces 3.39 GW. Finally, the overall cost for the Caltech SSPP is \$0.10-0.31/kWh, whereas the Proposed SSPP has an LCOE of \$1.06/kWh. The main differences in the final cost are due to the Proposed SSPP's use of today's costs and numbers that are accessible to the team.

References

[1] "Silicon Solar Space Cell S 32." http://www.azurspace.com/images/pdfs/0002162-00-03_DB_SIA.pdf. Accessed 04-18-2022.

[2] "TJ Solar Cell 3G30C - Advanced." http://www.azurspace.com/images/0003429-01-01_DB_3G30C-Advanced.pdf. Accessed 04-18-2022.

[3] "QJ Solar Cell 4G32C - Advanced." http://www.azurspace.com/images/0005979-01-01_DB_4G32C_Advanced.pdf. Accessed 04-18-2022.

[4] Solestial, "Thin film Silicon solar cell." https://solestial.com/cell/. Accessed 05-18-2022.

[5] W. Guter, F. Dunzer, L. Ebel, K. Hillerich, W. Kostler, T. Kubera, M. Meusel, B. Postels, and C. Wächter, "Space solar cells – 3g30 and next generation radiation hard products," 2017.

[6] M. A. Marshall, A. Goel, and S. Pellegrino, "Power-optimal guidance for planar space solar power satellites," *Journal of Guidance, Control, and Dynamics*, vol. 43, no. 3, pp. 518–535, 2020.

[7] P. Jaffe and J. McSpadden, "Energy conversion and transmission modules for space solar power," *Proceedings of the IEEE*, vol. 101, no. 6, pp. 1424–1437, 2013.

[8] E. Gdoutos, A. Truong, A. Pedivellano, F. Royer, and S. Pellegrino, "Ultralight deployable space structure prototype," 01 2020.

[9] Endurosat, "UHF Transceiver II CubeSat Communication." https://www.endurosat.com/cubesat-store/cubesat-communication-modules/uhf-transceiver-ii/. Accessed 05-27-2022.

[10] Rocket Lab, "Star Tracker ST-16RT2 Data Sheet." https://www.rocketlabusa.com/assets/Uploads/RL-ST16RT2-Data-Sheet.pdf. Accessed 05-27-2022.

[11] CubeSatShop, "NSS CubeSat Sun Sensor." https://www.cubesatshop.com/product/nss-cubesat-sun-sensor/. Accessed 05-27-2022.

[12] Minco Components, "HK6900— Polyimide Thermofoil™ Heaters." http://catalog.minco.com/catalog3/d/minco/?c=products&cid=3_1-polyimide-thermofoil-heaters&id=HK6900. Accessed 05-27-2022.

[13] Tesla, "Tesla Megapack." https://www.tesla.com/megapack/design. Accessed 05-11-2022.

[14] Peter O'Connor, "What Is the Learning Curve—and What Does It Mean for Solar Power and for Electric Vehicles?." https://blog.ucsusa.org/peter-oconnor/what-is-the-learning-curve/. Accessed 05-07-2022.

[15] C. A. Security, "Space Environment: Total Launches by Country." https://aerospace.csis.org/data/space-environment-total-launches-by-country/. Accessed 2022-04-17.

[16] John Mankins, "SPS-ALPHA: The First Practical Solar Power Satellite via Arbitrarily Large Phased Array." https://www.nasa.gov/directorates/spacetech/niac/mankins_sps_alpha.html. Accessed 04-20-2022.

[17] David C. Hyland, Haithem A. Altwaijry, "POWER START^{TM}: A NEW APPROACH TO SPACE SOLAR POWER." Accessed 04-26-2022.

[18] M. A. Marshall, R. G. Madonna, and S. Pellegrino, "Investigation of equatorial medium earth orbits for space solar power," *IEEE Transactions on Aerospace and Electronic Systems*, pp. 1–1, 2021.

[19] N. Fatemi, H. Pollard, H. Hou, and P. Sharps, "Solar array trades between very high-efficiency multi-junction and si space solar cells," in *Conference Record of the Twenty-Eighth IEEE Photovoltaic Specialists Conference - 2000 (Cat. No.00CH37036)*, pp. 1083–1086, 2000.

[20] G. Strobl, L. Ebel, D. Fuhrmann, W. Guter, R. Kern, V. Khorenko, W. Köstler, and M. Meusel, "Development of lightweight space solar cells with 30efficiency at end-of-life," in *2014 IEEE 40th Photovoltaic Specialist Conference (PVSC)*, pp. 3595–3600, 2014.

[21] E. Ralph, "High efficiency solar cell arrays system trade-offs," in *Proceedings of 1994 IEEE 1st World Conference on Photovoltaic Energy Conversion - WCPEC (A Joint Conference of PVSC, PVSEC and PSEC)*, vol. 2, pp. 1998–2001 vol.2, 1994.

[22] "Next Generation Upright Metamorphic 4-Junction Space Solar Cells." `https://artes.esa.int/projects/next-generation-upright-metamorphic-4junction-space-solar-cells`. Accessed 04-18-2022.

[23] M. Yamaguchi, S. Taylor, S. Matsuda, O. Kawasaki, and K. Ando, "Analysis of damage to silicon solar cells by high fluence electron irradiation," in *Conference Record of the Twenty Fifth IEEE Photovoltaic Specialists Conference - 1996*, pp. 167–170, 1996.

[24] J. J. P. James R. Wertz, David F. Everett, *Space Mission Analysis and Design: The new SMAD*. El Segundo, California: Microcosm Press, 2011.

[25] M. Yamaguchi, K.-H. Lee, K. Araki, N. Kojima, Y. Okuno, and M. Imaizumi, "Analysis for nonradiative recombination loss and radiation degradation of si space solar cells," *Progress in Photovoltaics: Research and Applications*, vol. 29, no. 1, pp. 98–108, 2021.

[26] P. Balaji, W. J. Dauksher, S. G. Bowden, and A. Augusto, "Flexible silicon heterojunction solar cells on 40 µm thin substrates," in *2019 IEEE 46th Photovoltaic Specialists Conference (PVSC)*, pp. 1089–1092, 2019.

[27] E. C. Warmann, P. Espinet-Gonzalez, N. Vaidya, S. Loke, A. Naqavi, T. Vinogradova, M. Kelzenberg, C. Leclerc, E. Gdoutos, S. Pellegrino, and H. A. Atwater, "An ultralight concentrator photovoltaic system for space solar power harvesting," *Acta Astronautica*, vol. 170, pp. 443–451, 2020.

[28] Saadah, Mohammed Ahmed, "Thermal Management of Solar Cells." `https://escholarship.org/uc/item/74t3m0b1#main`. Accessed 05-10-2022.

[29] SpaceX, "SpaceX Updates Page." `https://www.spacex.com/launches/`. Accessed 05-11-2022.

[30] ArianeGroup, "Ariane 5 User Handbook." `https://www.ariane.group/en/`. Accessed 05-11-2022.

[31] SpaceX, "Falcon User Handbook." `https://www.spacex.com`. Accessed 05-11-2022.

[32] Orbital ATK, "Geostar 2 bus datasheet." `https://satsearch.co/products/orbital-atk-geostar-2-bus-a-fully-redundant-flight-proven-spacecraft-bus-designed-for-geo` 2017. [Online; accessed 28-May-2022].

[33] A. Soni and H. B. Hablani, "Relative navigation of geo satellites in formation using double-difference carrier phase measurements with integer ambiguity resolution," in *2015 International Conference on Recent Developments in Control, Automation and Power Engineering (RDCAPE)*, pp. 50–54, 2015.

[34] Jeffrey Stuart, JPL, "Formation flying and position determination for a space-based interferometer in geo graveyard orbit." https://trs.jpl.nasa.gov/bitstream/handle/2014/47460/CL%2317-0971.pdf?sequence=1, 2017. [Online; accessed 28-May-2022].

[35] NASA Science, "Ion propulsion." https://solarsystem.nasa.gov/missions/dawn/technology/ion-propulsion/, 2018. [Online; accessed 28-May-2022].

[36] CS Hyde Company, "0.5 mil Kapton® Type HN Film." https://catalog.cshyde.com/item/films/kapton-polyimide-film-type-hn/18-5-24. Accessed 05-27-2022.

[37] DuPont, "DuPont™ Kapton® HN." https://catalog.cshyde.com/Asset/Data%20Sheet%2018-__F%20Dupont%20Kapton%C2%AE%20HN%20Film.pdf. Accessed 05-27-2022.

[38] PCBGOGO, "Flexible PCB Manufacturing — Low Cost FPC." https://www.pcbgogo.com/flexible-pcb-quote.aspx. Accessed 05-27-2022.

[39] Ritchie, Hannah, "The price of batteries has declined by 97% in the last three decades." https://ourworldindata.org/battery-price-decline. Accessed 05-27-2022.

[40] Eagle Picher Technologies, "High energy, long-cycle life and low maintenance lithium-ion cell for demanding applications." https://www.eaglepicher.com/sites/default/files/LP%2033081%2030Ah%20Space%20Cell%20%20040319.pdf. Accessed 05-27-2022.

[41] C. Montag, T. Schönherr, G. Herdrich, and J. Gonzalez del Amo, "Updates towards an automated vertical impulse pendulum and performance characterization of petrus 2.0," 05 2018.

[42] J. McSpadden, L. Fan, and K. Chang, "Design and experiments of a high-conversion-efficiency," 1998.

[43] U. Administration, *Nasa Cost Estimating Handbook Ver 4.0*. CreateSpace Independent Publishing Platform, 2017.

[44] K. Miura, "Method of packaging and deployment of large membranes in space," 1980.

A Launch envelope calculations

This section contains the first order calculations of how much space will the proposed design occupy during launch conditions. Considering 300 maximum launches possible and overall PV area in space to be $1.35km^2$, we get an area of $4500m^2$ per launch which comes out to be 67m side square. Now, considering Ariane-5 launch fairing specifications, we get a diameter of 5m to fit in the this area. We propose origami[44] based solution to tackle this problem. This methods folds a larger area square into small parallelograms. Side of each parallelogram can not exceed the payload fairing cross section. This gives 3.5m size of each parallelogram facet. Number of folds can be calculated is 67m(size of larger square) divided by size of each parallelogram i.e. 3.5m which comes out to be 19 folds in each direction. Considering thickness of the sandwich layer to be 0.04m gives a stacked thickness of 19x19x0.04= 14.4m.

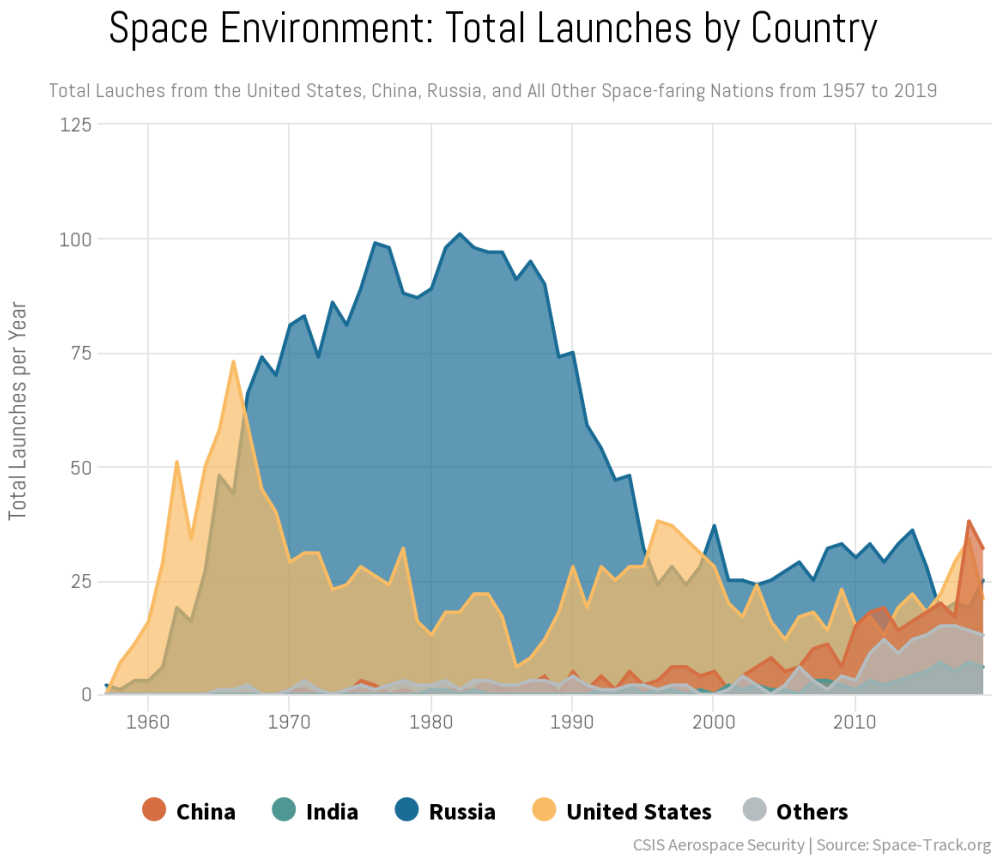

Figure 32: Launch numbers over time[15]

B Orbit Raising Propellant Mass Code

```
m0 = 903;
dv = 1.95422;
isp = 3100;

mf = m0 * exp(-dv/(0.00981 * isp));

mprop = m0 - mf;
```